

# VERY LARGE ARRAY OBSERVATIONS OF GALACTIC CENTER OH 1720 MHz MASERS IN SAGITTARIUS A EAST AND IN THE CIRCUMNUCLEAR DISK

LORÁNT O. SJOUWERMAN

National Radio Astronomy Observatory, 1003 Lopezville Rd., Socorro, NM 87801,

YLVA M. PIHLSTRÖM

Department of Physics and Astronomy, University of New Mexico, 800 Yale Boulevard NE, Albuquerque, NM 87131,

*Draft version October 19, 2018*

## ABSTRACT

We present Very Large Array (VLA) radio interferometry observations of the 1720 MHz OH masers in the Galactic Center (GC). Most 1720 MHz OH masers arise in regions where the supernova remnant Sgr A East is interacting with the interstellar medium. The majority of the newly found 1720 MHz OH masers are located to the northeast, independently indicating and confirming an area of shock interaction with the +50 km s<sup>-1</sup> molecular cloud (M-0.02-0.07) on the *far* side of Sgr A East. The previously known bright masers in the southeast are suggested to be the result of the interaction between two supernova remnants, instead of between Sgr A East and the surrounding molecular clouds as generally found elsewhere in the Galaxy. Together with masers north of the circumnuclear disk (CND) they outline an interaction on the *near* side of Sgr A East. In contrast to the interaction between the +50 km s<sup>-1</sup> cloud and Sgr A East, OH absorption data do not support a direct interaction between the CND material and Sgr A East. We also present three new high-negative velocity masers, supporting a previous single detection. The location and velocities of the high-negative and high-positive velocity masers are consistent with being near the tangent points of, and physically located *in* the CND. We argue that the high velocity masers in the CND are pumped by dissipation between density clumps in the CND instead of a shock generated by the supernova remnant. That is, the CND masers are not coupled to the supernova remnant and are sustained independently.

*Subject headings:* masers – Galaxy: center – ISM: individual (Sagittarius A East, Circumnuclear Disk, M-0.02-0.07) – galaxies: nuclei

## 1. INTRODUCTION

Two different types of masers are observed in the 1720 MHz satellite line transition of hydroxyl (OH); one is found in star forming regions (SFRs) and the other is associated with supernova remnants (SNRs). The radiatively pumped 1720 MHz masers in SFRs are accompanied by masers in the other ground-state rotational transitions (at 1612, 1665 and 1667 MHz) as a result of the cascade down from higher excitation levels, whereas the collisionally pumped 1720 MHz line is the only OH transition observed near SNRs (Lockett et al. 1999; Wardle 1999; Pihlström et al. 2008). The latter masers originate in post-shocked regions where an expanding SNR collides with dense molecular clouds in the surrounding interstellar medium (ISM), and are observed near SNR/ISM interaction regions throughout the Galaxy (e.g., Frail et al. 1994; Green et al. 1997). The Galactic center (GC) with the Sgr A East SNR plowing into the ISM surrounding the Sgr A Complex is no exception.

The line-of-sight toward the Sgr A Complex consists of the SNR Sgr A East and a circumnuclear disk (CND). Sgr A East manifests itself as a radio continuum ridge or shell (e.g., Ekers et al. 1983; Nord et al. 2004), in part obscured by the torus- or ring-like CND. The CND consists of irregularly distributed clumps of molecular gas (e.g., Jackson et al. 1993; Christopher et al. 2005) rotating counter-clockwise in a ring with a mean radius of about 2 pc around the compact radio source Sgr A\*, the dynamical center of the Milky Way (Reid & Brunthaler 2004). Interior to the CND, most gas

is ionized and is distributed in a “minispiral”, also known as the H II region Sgr A West. This line-of-sight also partly overlaps with two Giant Molecular Clouds (GMCs) casually called the +20 and +50 km s<sup>-1</sup> clouds (M-0.13-0.08 and M-0.02-0.07; see reviews in Morris & Serabyn 1996; Mezger et al. 1996). These form the “molecular belt” stretching across the Sgr A Complex, providing the ISM that interacts with Sgr A East.

It has long been known that a number of bright 1720 MHz masers with line-of-sight velocities near 50–65 km s<sup>-1</sup> are observed in the southwest region of Sgr A East, toward the SNR G359.02-0.09 (Ho et al. 1985; Coil & Ho 2000). A few other isolated masers are also distributed at other locations along the radio continuum shell with velocities between 40 and 60 km s<sup>-1</sup> (Yusef-Zadeh et al. 1996, hereafter YZ96; Karlsson et al. 2003, hereafter K03). In Sect. 4.3 we present new, less prominent 1720 MHz OH masers that are due to the interaction of Sgr A East and the +50 km s<sup>-1</sup> molecular cloud observed toward the northeast (e.g., Zylka et al. 1990; Ho et al. 1991; Tsuboi et al. 2006; Lee et al. 2008).

In addition, a few masers with very high absolute line-of-sight velocities can be found, at least in projection, near the CND (YZ96; K03; this work). Their high velocities (about +130 and -130 km s<sup>-1</sup>) do not fit the SNR/ISM interaction model. Instead, their signature resembles the structures of 1667 MHz OH and 22 GHz H<sub>2</sub>O masers found in circumnuclear tori of nearby galaxies (Miyoshi et al. 1995; Pihlström et al. 2001; Klöckner et al. 2003) suggesting that these masers arise in the CND itself. Until now this picture

TABLE 1

THE OBSERVING DATES, VLA BASELINE CONFIGURATION, CHANNEL SEPARATION  $\Delta V$ , TOTAL VELOCITY RANGE OBSERVED, TYPICAL  $1\sigma$  RMS NOISE LEVEL PER CHANNEL, SYNTHESIZED BEAM SIZE PLUS BEAM POSITION ANGLE FOR THE FOUR VLA DATA SETS AND REMARKS ON EACH DATA SET.

Date of observation	Config.	$\Delta V$ ( $\text{km s}^{-1}$ )	V-range ( $\text{km s}^{-1}$ )	Channel rms ( $\text{mJy beam}^{-1}$ )	Beam size & P.A. ( $'' \times ''$ at $^\circ$ )	Remarks
1986 Jun 30	BnA	8.5	-276 to +200	4	$5.2 \times 4.3$ , 10.4	Karlsson et al. (2003)
1996 Nov 22	BnA	2.1	-194 to +194	19	$7.1 \times 1.3$ , 39.8	Unpublished <sup>a</sup> part of Yusef-Zadeh et al. (1999)
1998 Jul 06	B	8.5	-276 to +200	3	$10.4 \times 4.4$ , 23.3	Previously unpublished archival data
2005 Jan 20 & 26	BnA	2.1	-232 to +232	3	$3.9 \times 3.6$ , -57.9	New observations

<sup>a</sup> Yusef-Zadeh et al. (1999) used two observational set-ups, only the narrow bandwidth high spectral resolution data were published in their paper.

for the GC depended on a previous single detection of a  $-132 \text{ km s}^{-1}$  maser. Section 4.4 presents support for this model with the detection of a number of new high-negative velocity masers.

In Sect. 2 and Sect. 3 we outline the data reduction procedures and present the results. In Sect. 4 the nature of the different groups of 1720 MHz masers in the GC is discussed. With this in mind, we present a model of the interaction of Sgr A East with its surroundings. Unless stated otherwise, all velocities in this paper refer to line-of-sight velocities as measured with respect to the Local Standard of Rest (LSR).

## 2. NEW OBSERVATIONS AND ARCHIVAL DATA

New high-sensitivity and high spatial resolution VLA observations were obtained to search for high-velocity masers in the CND. The new, 2005 January observations (Table 1) had two IF pairs of 1.562 MHz bandwidth, each tuned to slightly offset center velocities in order to cover a large total velocity range ( $-232 < V_{\text{LSR}} (\text{km s}^{-1}) < +232$ ). The data were calibrated using VLARUN, a pipeline VLA data reduction procedure available in NRAO's Astronomical Image Processing System (AIPS). After continuum subtraction in the UV-plane the data were imaged with natural weighting using standard AIPS procedures, very similar to the data reduction as described in K03. The only difference was that we joined the spectra from the two IF pairs into one long spectrum covering the whole velocity range with the higher spectral resolution using UJOIN. Self-calibration was performed using the bright  $+132 \text{ km s}^{-1}$  maser feature, which resulted in positional uncertainty of about  $0.2\text{--}0.3''$ . The resulting data cube has a synthesized beam full width half maximum (FWHM) of  $3''.9 \times 3''.6$  at a position angle (P.A.) of  $-57.9^\circ$ , and a channel separation of  $2.1 \text{ km s}^{-1}$  (i.e., a channel resolution of  $2.5 \text{ km s}^{-1}$ ). With dual polarizations and a total on-source integration time of about three hours, a typical rms noise of  $3.2 \text{ mJy beam}^{-1}$  per channel was achieved.

Three archival VLA data sets (out of which two are not published) have comparable velocity coverage, spatial resolution and sensitivity to the new observations and were re-analyzed following the same calibration procedure described above (see Table 1). They were included because we were interested in searching for the newly discovered masers in the older data sets (Sect. 3.1), and re-analyzed because such a search would be easier when using the same (self-calibration) reference peak. Since the masers typically are as narrow as a couple  $\text{km s}^{-1}$ , all masers in these archival data sets should have been re-detected in the new data set if the masers would not vary in flux. All archival data sets are in B1950 coordinates, and the new (2005 January) data set is in J2000 coordinates.

## 3. RESULTS

The observational results can be divided in two parts: point-like 1720 MHz (maser) emission and extended 1720 MHz absorption, presented in turn below.

### 3.1. 1720 MHz masers

To unambiguously exclude noise spikes as false maser detections, we consider a maser to be detected only if it has a channel flux density larger than 10 times the  $1\sigma$  rms noise level in its data set. With this strict constraint, we detect 13 new and 13 previously published masers in the 2005 data. One of the newly discovered masers was also detected in the 1998 data (maser #1 in Table 2 at  $11\sigma$ ) but no other new masers were found above  $10\sigma$  in the archival VLA data. Apart from the general possibility of intrinsic variability (which exists: Sect. 4.4), this is most likely due to the much larger channel widths ( $8.5 \text{ km s}^{-1}$ ) or the much larger rms noise in the archival data sets. For example, assuming no variability, the brightest new single-channel detection (maser #24 at  $25\sigma$ ) would be smeared to less than  $7\sigma$  rms in a  $8.5 \text{ km s}^{-1}$  channel in the 1986 June data set and thus would remain undetected using our strict  $10\sigma$  constraint. Actually, knowing the positions and velocities of the newly detected masers, we found most of the masers #20–28 at about  $4\sigma\text{--}6\sigma$  levels back in both the 1986 and 1998 data; the 1996 data was too noisy. Also maser #6 was found in the archival data, but at  $7\sigma$  in the 1998 data only; it had not appeared in 1986 and apparently weakened since 1998. Two previous detections (masers #4 and #19 in Table 2) were not detected (down to  $4\sigma$ ) in the 2005 data but are included in Table 2 for the completeness of the discussion in this paper.

Table 2 lists the OH name in galactic coordinates, the position of the maser, the total width in  $\text{km s}^{-1}$  of the channels in which emission occurs, the velocity of the channel containing the peak flux, the total detected flux integrated over the velocity width, and finally references to the papers where previous detections are reported. For the masers detected multiple times, we have adopted the parameters derived from the most recent 2005 dataset, or from K03 if the maser was confused or undetected in 2005 (for confusion see Yusef-Zadeh et al. 1999). Small positional offsets compared to earlier papers are due to differences in the self-calibration. Velocity offsets and flux differences are due to different observing parameters per data set and possible intrinsic variability of the maser. Because the maser emission is generally found only in 1-2 channels and may be non-Gaussian and narrower than the channel separation, spectral fitting to the feature to obtain a fitted flux, center velocity, FWHM and their associated errors is meaningless. We therefore assume an uncertainty in the center velocity and velocity range of half the channel separation (i.e., 1

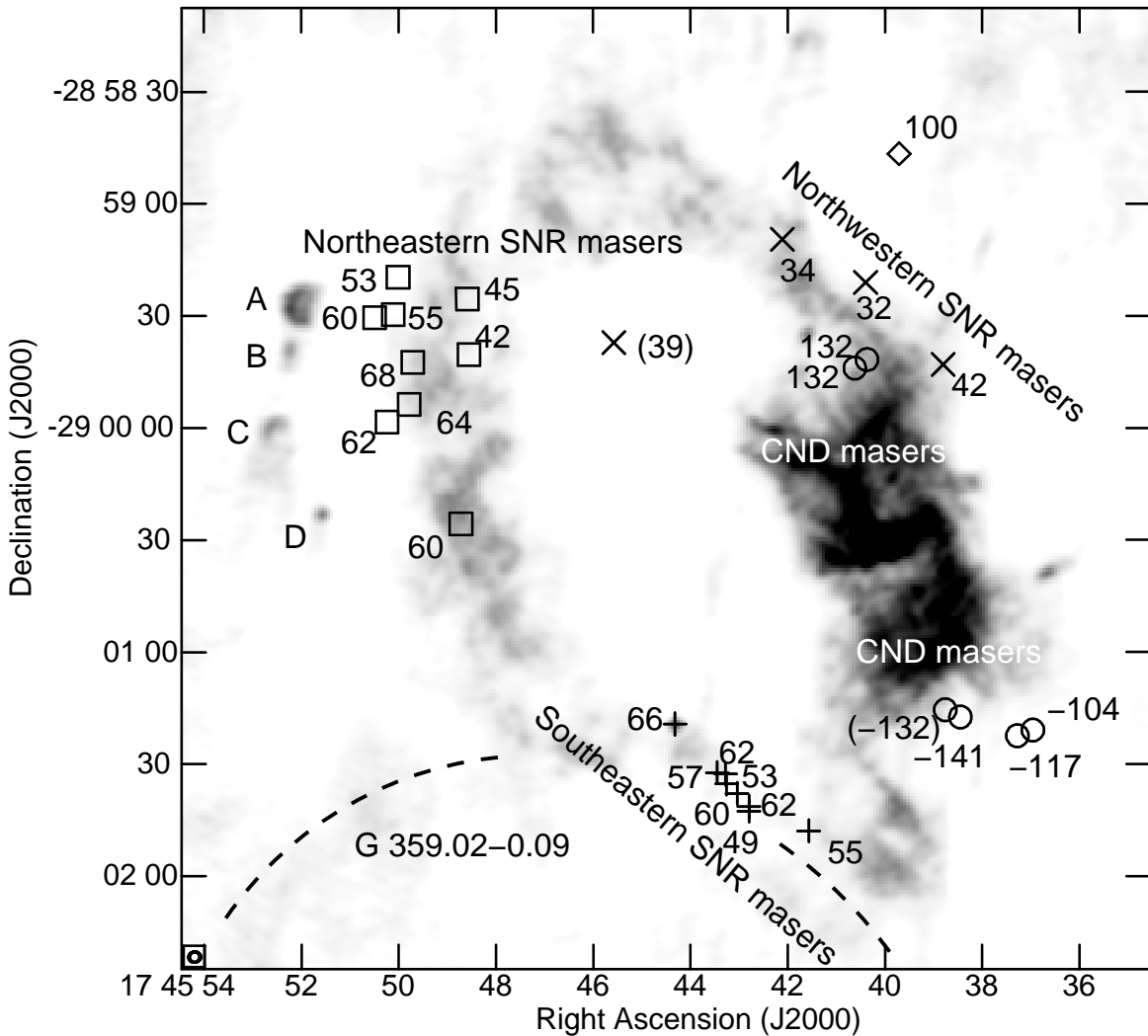


FIG. 1.— Location of the 1720 MHz OH masers with respect to Sgr A East (ring-like structure) and the CND and minispiral (dark S-like spiral on the right). The masers are superimposed on the 1.7 GHz radio continuum created from the frequency averaged 2005 January data. Numbers associated with symbols are the maser LSR velocities. Squares, crosses and pluses denote masers associated with the SNR shell (i.e., the northeastern, northwestern and southeastern SNR masers, respectively), circles are masers associated with the CND. The diamond represents another newly detected maser. All masers in the upper left (squares, northeastern SNR masers) except the  $+55 \text{ km s}^{-1}$  one are newly found masers. Two masers from Karlsson et al. (2003) with velocities in parentheses are not re-detected in the data after 1986. The molecular belt roughly stretches with increasing velocity from the lower right corner to the upper left corner. The dotted semi-circle outlines the SNR G359.02–0.09 and labels A–D identify H II regions (see Sect. 4.3).

$\text{km s}^{-1}$  except for the ones adopted from K03 where it is about  $4 \text{ km s}^{-1}$ ), and up to 50% uncertainty in the flux. The flux values given should therefore be regarded as indicative for their relative intensity only. Good fits and associated errors can be obtained with new high spectral resolution observations, e.g. as in Yusef-Zadeh et al. (1999), but this is beyond the scope of this paper.

Figure 1 shows the masers from Table 2 labeled with their velocities on top of a gray scale 1.7 GHz radio continuum image made from the frequency averaged 2005 data. Two different populations of masers can be identified: a) masers with velocities between  $+30$  and  $+70 \text{ km s}^{-1}$  following the outline of the Sgr A East SNR shell (“SNR masers”, marked with squares, crosses and pluses), and b) masers with absolute velocities  $> 100 \text{ km s}^{-1}$  which are consistent with velocities of the CND at their projected position (“CND masers”, circles). Note that the latter are located in projection, not only on top and near the CND, but also on top and near the Sgr A East

SNR shell, albeit with a distinct high velocity. One additional new maser (at  $+100 \text{ km s}^{-1}$ ) seems distinct from the two main populations (diamond, Sect. 4.3.1).

We find a significant number (3) of new high-negative velocity masers toward the southwestern part of the CND (circles in Fig. 1), but no new high-positive velocity masers. The CND masers are only found near the tangent points<sup>1</sup> of the torus-like and inclined CND, suggesting that the masers are found only there due to the longer path-length (Pihlström et al. 2001; Parra et al. 2005, see Sect. 4.4.2). Furthermore, almost all new SNR masers are found toward the northeastern rim of the SNR shell, in projection close to the

<sup>1</sup> Assuming an inclined circular torus, the tangent points are the narrowest part at the ends of the major axis of the projected ellipse on the sky. These are also the regions where the projected column densities, and thus also the path-lengths for maser gains, are highest (Parra et al. 2005), and where limb-brightening of a homogeneously emitting torus occurs (Yusef-Zadeh et al. 2001).

TABLE 2  
1720 MHz OH MASERS DETECTED IN THE SGR A COMPLEX.

No	OH Name ( <i>l, b</i> )	Position in B1950 (RA & Dec B1950)		Position in J2000 (RA & Dec J2000)		$\Delta V^a$ ( $\text{km s}^{-1}$ )	$V_{\text{sys}}$	Flux (Jy)	Ref. <sup>b</sup>
1	359.925–0.044	17 42 26.21	–29 00 11.2	17 45 36.96	–29 01 20.9	4.2	–104	0.11	
2	359.926–0.045	17 42 26.53	–29 00 12.7	17 45 37.28	–29 01 22.4	2.1	–117	0.05	
3	359.929–0.048	17 42 27.70	–29 00 07.7	17 45 38.45	–29 01 17.4	2.1	–141	0.04	
4 <sup>c</sup>	359.930–0.048	17 42 28.02	–29 00 05.8	17 45 38.76	–29 01 15.5	8.5 <sup>c</sup>	–132	0.07	1,2
5	359.952–0.035	17 42 28.10	–28 58 33.4	17 45 38.80	–28 59 43.0	4.2	42	0.62	1,3
6	359.967–0.030	17 42 29.02	–28 57 37.0	17 45 39.71	–28 58 46.6	2.1	100	0.04	
7 <sup>c</sup>	359.955–0.040	17 42 29.67	–28 58 32.2	17 45 40.37	–28 59 41.7	8.5 <sup>c</sup>	132	0.29	1,3
8	359.960–0.037	17 42 29.71	–28 58 11.6	17 45 40.40	–28 59 21.1	4.2	32	0.15	1
9 <sup>c</sup>	359.955–0.041	17 42 29.91	–28 58 34.4	17 45 40.62	–28 59 44.0	8.5 <sup>c</sup>	132	0.66	1,3
10	359.928–0.062	17 42 30.81	–29 00 38.5	17 45 41.57	–29 01 47.9	6.3	55	0.51	1,3
11	359.966–0.041	17 42 31.41	–28 58 00.1	17 45 42.11	–28 59 09.5	2.1	34	0.03	
12 <sup>d</sup>	359.932–0.065	17 42 32.04	–29 00 32.1	17 45 42.80	–29 01 41.4	4.2	62	0.10	1,3
13 <sup>d</sup>	359.931–0.065	17 42 32.05	–29 00 33.2	17 45 42.80	–29 01 42.6	2.1	49	0.09	1,3
14 <sup>d</sup>	359.933–0.065	17 42 32.28	–29 00 28.5	17 45 43.04	–29 01 37.9	2.1	60	0.10	1,3
15 <sup>d</sup>	359.934–0.065	17 42 32.51	–29 00 26.0	17 45 43.26	–29 01 35.3	4.2	53	0.40	1,3
16 <sup>d</sup>	359.935–0.065	17 42 32.53	–29 00 23.4	17 45 43.28	–29 01 32.7	4.2	62	0.24	1,3
17 <sup>d</sup>	359.935–0.065	17 42 32.69	–29 00 22.9	17 45 43.45	–29 01 32.2	4.2	57	0.60	1,3
18	359.940–0.066	17 42 33.57	–29 00 10.0	17 45 44.32	–29 01 19.3	6.3	66	6.07	1,3
19 <sup>c</sup>	359.966–0.055	17 42 34.88	–28 58 28.0	17 45 45.58	–28 59 37.2	8.5 <sup>c</sup>	39	0.08	1
20	359.971–0.065	17 42 37.84	–28 58 31.4	17 45 48.55	–28 59 40.4	2.1	42	0.03	
21	359.975–0.063	17 42 37.89	–28 58 16.6	17 45 48.59	–28 59 25.5	4.2	45	0.10	
22	359.961–0.072	17 42 37.99	–28 59 16.8	17 45 48.72	–29 00 25.7	2.1	60	0.03	
23	359.973–0.069	17 42 39.00	–28 58 33.6	17 45 49.71	–28 59 42.4	4.2	68	0.18	
24	359.970–0.071	17 42 39.07	–28 58 44.8	17 45 49.78	–28 59 53.7	2.1	64	0.08	
25	359.979–0.067	17 42 39.31	–28 58 10.8	17 45 50.01	–28 59 19.6	2.1	53	0.06	
26	359.977–0.068	17 42 39.41	–28 58 20.8	17 45 50.11	–28 59 29.7	2.1	55	0.04	1
27	359.970–0.073	17 42 39.52	–28 58 49.6	17 45 50.24	–28 59 58.4	2.1	62	0.06	
28	359.977–0.070	17 42 39.78	–28 58 21.7	17 45 50.49	–28 59 30.5	2.1	60	0.05	

<sup>a</sup> The velocity width is the total velocity range of the channels in which maser emission occurs.

<sup>b</sup> References: 1) Karlsson et al. (2003), 2) Yusef-Zadeh et al. (2001) (using the same data as Karlsson et al. 2003), 3) Yusef-Zadeh et al. (1996).

<sup>c</sup> Parameters adopted from Karlsson et al. (2003); the  $\Delta V$  of  $8.5 \text{ km s}^{-1}$  is an upper limit due to the large channel separation used.

<sup>d</sup> Maser complex #12–17 corresponds to maser 7 in Karlsson et al. (2003) and D, E, and F in Yusef-Zadeh et al. (1996).

H II regions A–D (that lie in front of the  $50 \text{ km s}^{-1}$  cloud), and close to where the deepest 1667 MHz OH absorption occurs (K03). As these masers are much weaker than the masers toward G359.02–0.09 in the southeast (e.g., YZ96), they have not been detected in previous observations other than a single one in K03. It is in this region that Ho et al. (1991) and, more recently, Lee et al. (2003) and Tsuboi et al. (2006) have detected signs of shock interactions using observations of  $\text{NH}_3$ ,  $\text{H}_2$  and CS emission (Sect. 4.3).

### 3.2. 1720 MHz OH distribution

Although individual clumps and streamers do confuse and complicate the overall interpretation, our 1720 MHz OH absorption maps are completely consistent with the conclusions drawn by K03 and others (e.g. Pedlar et al. 1989; Sandqvist 1989; Zylka et al. 1990). That is, *i*) part of the distribution of the +20 and +50  $\text{km s}^{-1}$  clouds is located *in front of* the Sgr A East SNR shell, *ii*) the CND must be located on the near side of Sgr A East, and, *iii*) the +20  $\text{km s}^{-1}$  and +50  $\text{km s}^{-1}$  clouds must be *mostly behind* Sgr A\* and the minispiral, thus behind the CND.

The large scale absorption distribution illustrates conclusion *i*) above. Figure 2 plots selected velocity maps of the 1720 MHz OH absorption superimposed on the radio continuum where each panel displays spectrally smoothed absorption with a width of  $21.7 \text{ km s}^{-1}$ . It resembles the on-line

material by K03 (their Fig. 4), but is included here as it shows the large extent of the 1720 MHz absorption more clearly than in K03. Figure 2 demonstrates that the large scale absorption at +58 to +36  $\text{km s}^{-1}$  occurs in the eastern part of the SNR shell, while absorption at lower velocities (+36 to +14  $\text{km s}^{-1}$ ) also covers the western part of the shell, consistent with *i*). Further, the K03 data as well as our absorption data (not shown here; see Pihlström & Sjouwerman 2006) reveal the CND in absorption at high absolute velocities ( $\sim 100$ – $150 \text{ km s}^{-1}$ ) at opposing azimuth angles of the CND major axis, thus concluding *ii*). Finally, our data confirm that the minispiral and Sgr A\* are devoid of absorption. We refer to K03 (their Sect. 3.1.1) for discussing the lack of absorption in detail, but note that our results support that the general lack of absorption toward Sgr A\* and the minispiral therefore imply *iii*).

## 4. DISCUSSION

The discussion concentrates on the nature of the 1720 MHz maser emission, detected at multiple spatial locations in the GC region. However, the absorption measurements play an important role in untangling the 3D structure of the region and the origin of the different groups of masers observed.

### 4.1. Structure of the GC region

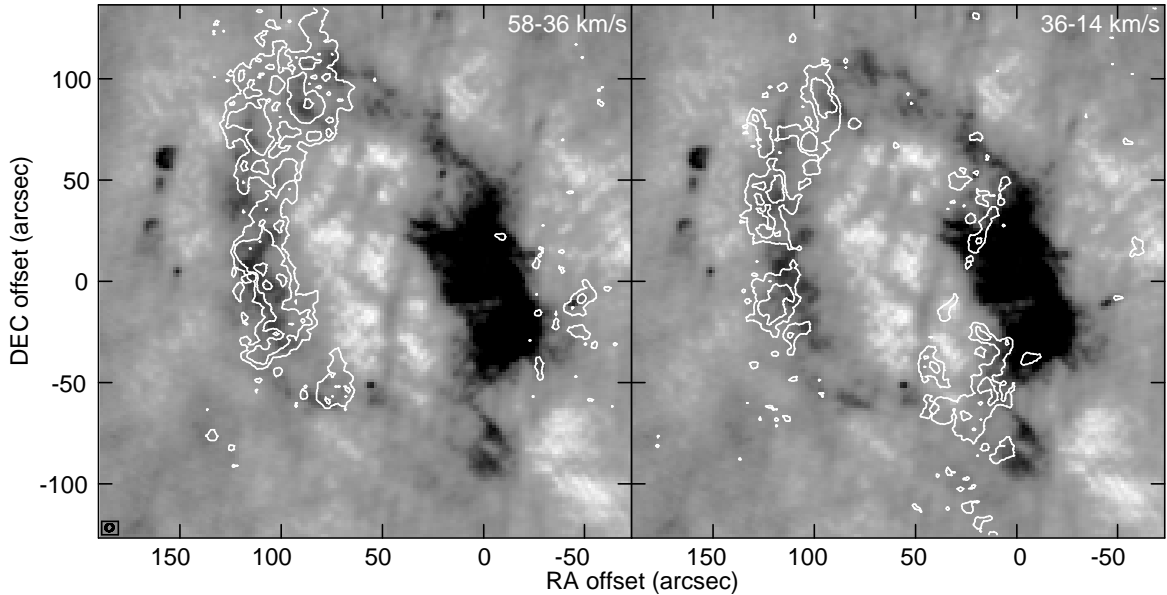


FIG. 2.— Spectrally smoothed 1720 MHz OH absorption at velocities between 58–36 and 36–14  $\text{km s}^{-1}$ . The data was smoothed to improve the signal to noise ratio. The absorption is shown in contours at 7.5, 15 and 22.5  $\text{mJy beam}^{-1}$ , superimposed on the gray scale image of a 1.7 GHz radio continuum. The offsets are with respect to Sgr A\*. These absorption maps centered at +46 and +25  $\text{km s}^{-1}$  illustrate the extent of the +20 and +50  $\text{km s}^{-1}$  clouds better than Karlsson et al. (2003). No absorption is observed toward Sgr A\* or the inner part of the CND (the minispiral). See Pihlström & Sjouwerman (2006) for our absorption results over the full velocity range of the CND.

Our absorption measurements corroborate the absorption results and conclusions of K03: parts of the molecular clouds must be *between* the CND in the front, and the SNR in the back (Sect. 3.2, Sect. 4.4). Previously, the location of the components in the line-of-sight toward the Sgr A Complex have been subject to different interpretations, in particular the line-of-sight location of the CND, the molecular cloud material and the Sgr A East SNR. Many authors (e.g., Güsten et al. 1981; Ho et al. 1985; Zylka et al. 1990; Ho et al. 1991; Marshall et al. 1995; Coil & Ho 2000; McGary et al. 2001; Karlsson et al. 2003; Vollmer et al. 2003; Christopher et al. 2005; Herrnstein & Ho 2005; Tsuboi et al. 2006) have tried to picture a three-dimensional (3D) model of the different components and structures. The latest is presented by Lee et al. (2008), who prefer a model where the Sgr A East SNR directly pushes against the CND. A slab of compressed molecular (or atomic) material might be a part of this interaction, but would not necessarily separate the SNR from the CND physically. This model is mostly based on larger velocity dispersions and lower velocity centroids in selected  $\text{H}_2$  emission slit observations, as compared to what is observed for the  $\text{NH}_3$  density clumps (e.g., Ho et al. 1991; Coil & Ho 2000; Herrnstein & Ho 2005). However, this does not directly imply that the SNR pushes the CND toward the observer, as indicated by Lee et al. (2008). It does indeed mean that the  $\text{H}_2$  gas is hotter, but it might as well be part of a different kinematic structure.

Since Sandqvist (1970, 1974), it is clear that with the many observations and interpretations of the Sgr A East Complex using different tracers and methods over the past  $\sim 40$  years, a full review with perhaps more sensitive (re)observations and/or minute re-interpretations of the available data and facts is needed to explain the structure. That is beyond the scope of this paper, as here we just want to explain the nature of the 1720 MHz OH masers, but we note that the full 3D structure still is not completely clear. A 3D model should also be

based on information from absorption lines which yields direct information of the line-of-sight location of the absorbing gas with respect to the background continuum. We therefore endorse the result of K03, that the Sgr A East SNR and the CND do not necessarily physically interact, since part of the molecular material lies between them.

#### 4.2. Origin of the 1720 MHz masers in the Sgr A Complex

Maser emission is primarily constrained by the narrow range of physical parameters required (Sect. 4.4.2). The amplification and population inversion of the 1720 MHz OH line requires number densities of the order of  $n_{\text{OH}} \sim 10^5 \text{ cm}^{-3}$ , temperatures in the range  $T = 50\text{--}125 \text{ K}$  and OH column densities of  $N_{\text{OH}} \sim 10^{16}\text{--}10^{17} \text{ cm}^{-2}$  (Elitzur 1976; Gray et al. 1991, 1992; Pavlakis & Kylafis 1996; Lockett et al. 1999; Pihlström et al. 2008). Such conditions can be found in SFRs (Palmer et al. 1984; Baudry et al. 1988; Gray et al. 1991, 1992; Cohen et al. 1995; Niezurawska et al. 2004) and in the post-shock regions near SNRs (Frail et al. 1994; Green et al. 1997; Wardle 1999).

Modeling of SNR/ISM interactions show that C-type shocks provide the required inverted OH column densities. However, in this paper we argue that some masers arise in non-standard locations, i.e., in the CND (Sect. 4.4). An independent check on whether this is reasonable can be made by estimating the OH column density in regions where masers occur, using the absorption data. In local thermal equilibrium (LTE)

$$N_{\text{OH}} = 1.96 \times 10^{15} T_{\text{ex}} \Delta V_{\text{FWHM}} \tau_{\text{peak}} \text{ cm}^{-2} \quad (1)$$

where  $T_{\text{ex}}$  is the excitation temperature in K,  $\Delta V_{\text{FWHM}}$  is the FWHM line width in  $\text{km s}^{-1}$  and  $\tau_{\text{peak}}$  is the 1720 MHz peak optical depth. The opacity is dependent on the absorbed flux density as well as the flux density of the background continuum. Since it is difficult to properly separate the different

continuum components (SNR shell, thermal emission from the ionized gas and non-thermal emission from Sgr A\*) and their location relative to the absorbing gas, the first order estimates given below are apparent opacities given for the assumed, simplest case with all absorbing gas in front of the continuum (see K03 for  $-T_L/T_C$  maps). Another caveat is, of course, that the OH is not likely to obey LTE conditions in these regions.

To estimate a typical column density toward the SNR shell, a (northeastern) region centered on  $\Delta RA = 75''$  and  $\Delta Dec = 104''$  was chosen. Here, the absorption feature has a velocity centroid close to  $+50 \text{ km s}^{-1}$  thus corresponding to gas in which the SNR/ISM masers arise. A single-component Gaussian fit yields an opacity of  $0.7 \pm 0.2$ ,  $\Delta V_{\text{FWHM}} = 15 \pm 3 \text{ km s}^{-1}$  and an OH column density  $N_{\text{OH}} = 2.2 \pm 0.7 \times 10^{16} T_{\text{ex}} \text{ cm}^{-2}$ , which are typical values in other regions toward the Sgr A East shell. Similarly, the OH column density of the CNL is estimated at a position centered at  $\Delta RA = -18''$  and  $\Delta Dec = 8''$ . To ensure the CNL opacity is measured excluding absorption from the molecular belt, a line with a centroid velocity of  $98 \text{ km s}^{-1}$  was used, resulting in  $\Delta V_{\text{FWHM}} = 31 \pm 3 \text{ km s}^{-1}$ , an opacity of  $0.5 \pm 0.1$  and an OH column density of  $N_{\text{OH}} = 2.7 \pm 0.7 \times 10^{16} T_{\text{ex}} \text{ cm}^{-2}$ . Compared to the SNR/ISM interaction sites, the line widths appear broader in the CNL, or alternatively consist of a larger number of overlapping components in velocity. Overall, we deduce that the estimated OH column densities in the CNL and in the SNR/ISM are similar, providing similar column density conditions.

The expected temperatures of 50-125 K can be combined with our estimate of the column density in the CNL,  $N_{\text{OH}} \simeq 2 \times 10^{16} T_{\text{ex}} \text{ cm}^{-2}$  (Sect. 3.2). The resulting observed column density is an order of magnitude larger than the  $N_{\text{OH}} \sim 10^{16} - 10^{17} \text{ cm}^{-2}$  predicted by 1720 MHz maser theories for regions with number densities of  $10^5 \text{ cm}^{-3}$ . However, this is not necessarily a contradiction, since the masers only occur in regions where the number density is constrained to  $n_{\text{OH}} \sim 10^5 \text{ cm}^{-3}$ . In regions with number densities above this value (reflected in an increased column density) maser emission will be quenched, perhaps in favor of 1612 MHz emission (Pihlström et al. 2008), and the gas will be observed in absorption instead. We note that Pihlström et al. (2008) do comment on 1612 MHz emission toward Sgr A East, but none is detected toward the CNL.

#### 4.3. The SNR masers

This subsection discusses the SNR masers found in the +30 to  $+70 \text{ km s}^{-1}$  velocity range; first the new and previously known masers in the northwest (crosses in Fig. 1), then the newly found masers in the northeast (squares), and finally the previously known masers in the southeast (plusses).

##### 4.3.1. Northwestern SNR masers

The masers to the northwest, north of the CNL, appear related to linear filaments traced by  $\text{H}_2$  emission (usually presumed to trace shocked, dense gas with  $n \sim 10^5 \text{ cm}^{-3}$ ). The positional coincidence of masers and  $\text{H}_2$  filaments was first noted by Yusef-Zadeh et al. (2001, hereafter YZ01), who used NICMOS observations to compare the position of the  $+42 \text{ km s}^{-1}$  maser (#5, YZ96) with the distribution of  $\text{H}_2$  line emission. The maser was found co-located with an  $\text{H}_2$  filament labeled the Linear Filament. In Fig. 3 we overplot the same  $\text{H}_2$  map with all masers. We note that the  $+32 \text{ km s}^{-1}$  maser (#8,

K03) is projected along the same Linear Filament as maser #5, and that the new  $+100 \text{ km s}^{-1}$  maser (#6) is located just north of another filament, called the Outer Filament. The position and velocity of the  $+100 \text{ km s}^{-1}$  maser may indicate that it is related to the  $+70 \text{ km s}^{-1}$  cloud (Gatley et al. 1986) or to the NW Extended Dark Cloud, but no  $\text{H}_2$  velocity information is available for this cloud for comparison (YZ01).

YZ01 suggest that the  $\text{H}_2$  filaments could be generated by the impact of Sgr A East into the backside of the CNL. As a note of caution, they also point out that this region is confused by the presence of the  $+70 \text{ km s}^{-1}$  cloud and the NW Extended Dark Cloud, either of which may be falling into the CNL from the foreground (Gatley et al. 1986; Jackson et al. 1993; Marshall et al. 1995; YZ01; K03). YZ01 base their interpretation on a spatial alignment of the Linear Filament with the western boundary of the SNR radio continuum ridge. A similar alignment can, however, also be argued with the NW Extended Dark Cloud. Thus, the suggestion that the  $\text{H}_2$  filaments are produced by a direct impact between Sgr A East and the CNL seems viable but, at this point, lacks unambiguous evidence.

To explain the appearance of the  $\text{H}_2$  filaments across the whole eastern part (including the Linear Filament, the Outer  $\text{H}_2$  clumps, and the filament west of the Southern Lobe) in connection to the masers in this region, we postulate an alternative model where the SNR triggers a shock in something much larger than the CNL. This model is depicted in the lower right inset of Fig. 3. Such an arc-like interaction model (outlined by the elliptical band in Fig. 3) would argue in favor of an impact of Sgr A East into more widespread molecular material, located between the SNR and the CNL. This interaction could, but would not necessarily have to shock the CNL.

As mentioned before, line emission observations (whether from  $\text{H}_2$  or  $\text{NH}_3$  gas, or OH masers) alone do not allow a proper line-of-sight determination of the different components — we are looking forward to e.g. absorption and/or extinction measurements toward these  $\text{H}_2$  filaments and  $\text{H}_2$  clumps. For now, we can state that the  $\text{H}_2$  emission filaments are consistent with *any* of these interpretations: *a*) Sgr A East is interacting with the CNL, *b*) Sgr A East is interacting with the  $+20/50 \text{ km s}^{-1}$  cloud in between the SNR and the CNL, or *c*) the  $\text{H}_2$  filaments are not due to an interaction with Sgr A East but due to an interaction with the NW Extended Dark Cloud or the  $+70 \text{ km s}^{-1}$  cloud. Nevertheless, with the absorption data available, and a model as shown in Fig. 3 (lower right panel), we favor alternative *b*) where these northwestern SNR masers are generated in the molecular cloud material at the front (near) side of the SNR. We cannot determine whether the shock does, or does not penetrate the CNL from the back.

##### 4.3.2. Northeastern SNR masers

One maser excepted, the group of weaker masers in the northeastern part of Sgr A East are all new detections. These masers appear situated near the well known ultra compact H II regions located farther east of the SNR (A, B, C, & D; Ho et al. 1985). Therefore, these northeastern masers could be associated with star formation, similar to what is observed in SFRs (Niezurawska et al. 2004; Szymczak & Gérard 2004). Relative to the SNR however, the H II regions are in the foreground (K03). Furthermore, the spatial spread and velocity distribution of the masers follow the “backward C” shape observed in  $\text{NH}_3$  by Ho et al.

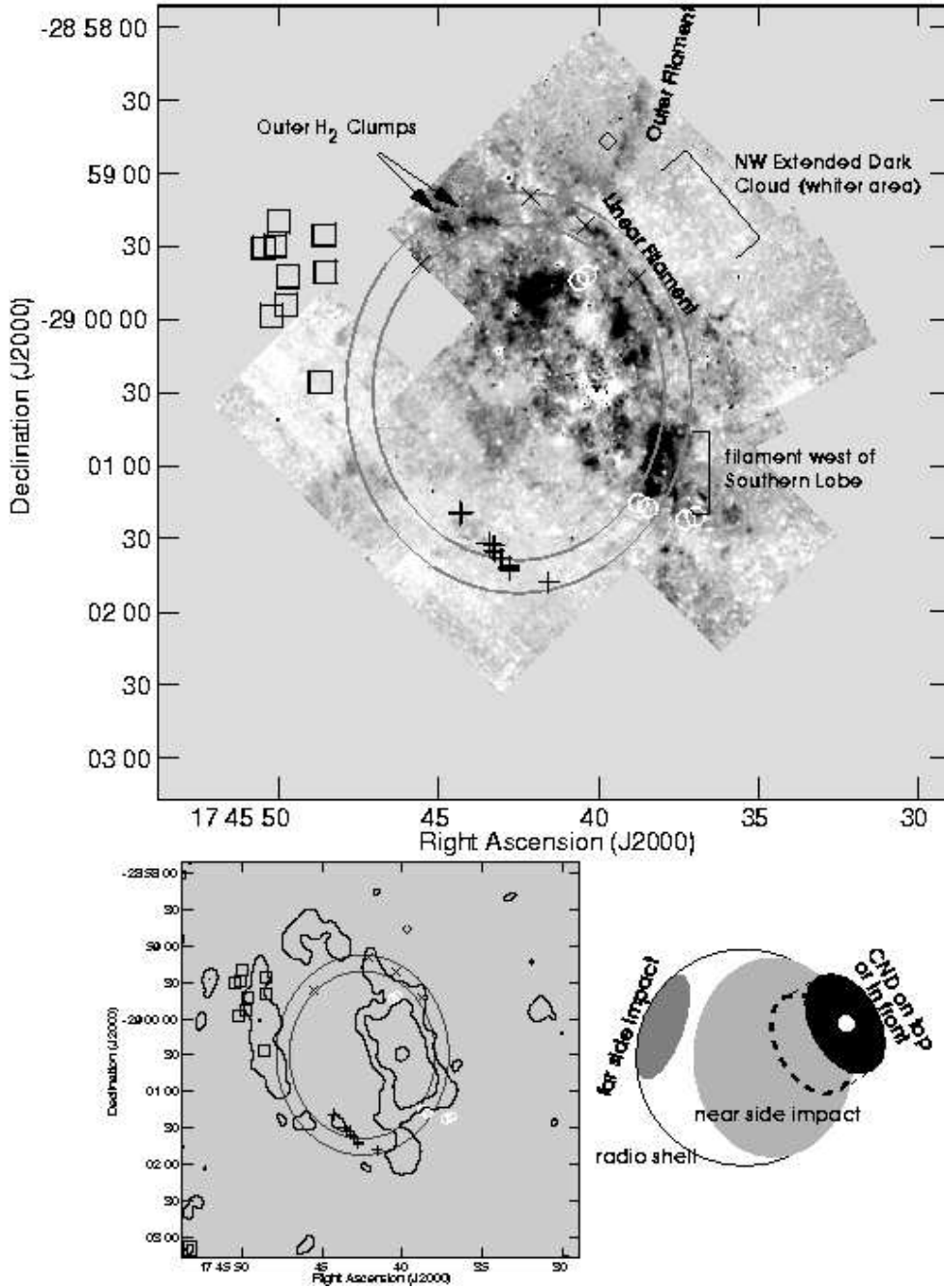


FIG. 3.— *Top*: Indicators of shock-excited material – 1720 MHz maser positions overlaid on the H<sub>2</sub> map of Yusef-Zadeh et al. (2001). Symbols as in Fig. 1. The northwestern masers (crosses) can suggestively be fitted with a (partial) band (between the gray ellipses) that includes the near side shock excited regions north and west of the CND traced by the H<sub>2</sub> filaments described by Yusef-Zadeh et al. (2001) (their Fig. 2b; see text). The southeastern masers (pluses) suggestively would also fit if the SNR G359.02–0.09 (Fig. 1) would not have pushed them inward, toward the northwest. *Lower left*: A redisplay of Fig. 1 as a contour map without labels but with the elliptical band for comparison. Note that the radio continuum shell is larger than the elliptical band; the radio continuum covers the northeastern masers (squares) at the far side impact. *Lower right*: A schematic model of Sgr A East interacting at the near side (light gray filled ellipse) and at the far side (dark gray filled ellipse). The black filled ellipse and the white dot depict the CND and Sgr A\*. Whether the elliptical band locating the region of interaction on the near side is complete or not, it depicts that the near side interaction region is larger than the size of the CND. We cannot determine whether the CND touches the near side impact region or not, only that it is located on its front side. The Southern Lobe of the CND overlaps with the elliptical band confusing the picture; it incorrectly suggests that the two CND masers (white circles) in projection seen in the band are also due to the interaction.

(1991) with the most red-shifted maser velocities in the center of the distribution. This combination thus depicts the shell-like interaction of the back<sup>2</sup> side of the Sgr A East SNR plowing into the +50 km s<sup>-1</sup> cloud and propagating away from the observer. This interaction and morphology has been described previously by many authors and indeed also implies that part of the +50 km s<sup>-1</sup> cloud is behind Sgr A East (e.g. Whiteoak et al. 1974; Sandqvist 1989; Zylka et al. 1990; Ho et al. 1991; Lee et al. 2008). This part of the +50 km s<sup>-1</sup> cloud behind the SNR has also been referred to as the (eastern part of the) Sgr A East core (Zylka et al. 1990; Mezger et al. 1996). The detection of the 1720 MHz OH masers independently confirms that there is such an interaction region and that the excitation mechanism for the observed H<sub>2</sub> emission is indeed due to a C-type shocked front (Lee et al. 2003, 2008). Unfortunately, H<sub>2</sub> filaments cannot be recognized in their slit observations (Sect. 4.3.1). In summary, we conclude that the northeastern SNR masers are generated in the molecular cloud material at the back (far) side of the SNR.

#### 4.3.3. Southeastern SNR masers

The previously reported bright SNR masers were all detected in our observations (YZ96; YZ01; K03). Those are the bright masers near the southeastern edge of Sgr A East (Fig. 1). The near-linear distribution of the masers in the southeast differs from the more spread-out spatial distribution of the masers to the northeast (Sect. 4.3.2). In the southeast corner of Fig. 1, an  $\sim 80''$ -radius semicircular weak continuum feature can be discerned. This continuum emission outlines another SNR shell, G359.02–0.09 (e.g., Coil & Ho 2000; Herrnstein & Ho 2005). Sakano et al. (2003) have detected non-thermal X-ray emission from parts of the G359.02–0.09 shell, with a spectrum that suffers large absorption consequently placing the X-ray source in the GC. In the sky, the G359.02–0.9 SNR shell overlaps the Sgr A East continuum, and is likely responsible for the inward-concave morphology of the southeastern Sgr A East shell (Coil & Ho 2000). This is precisely where the bright 1720 MHz masers form. In contrast to the northwestern masers, the NICMOS image only shows weak extended H<sub>2</sub> emission, no filaments (Fig. 3; YZ01). Moreover, this region displays almost no continuum background and OH absorption (Fig. 2; Fig. 3; K03). This region likely is a result of two colliding shock fronts and would explain why there is such a sharp line of bright masers. Previous discussions of these masers suggested that they are the result of the interaction of the +50 km s<sup>-1</sup> cloud and Sgr A East. We here suggest that they probably are due to a SNR/SNR interaction (albeit close to the front-side SNR/ISM interaction in Fig. 3), for which 1720 MHz maser emission has not been anticipated before.

#### 4.4. The CND masers

We here discuss the masers near the tangent points of the CND with high absolute ( $\pm 104$ – $141$  km s<sup>-1</sup>) velocities (circles in Fig. 1).

##### 4.4.1. Origin and variability of the CND masers

A bright maser at +132 km s<sup>-1</sup> has been detected in all observations (i.e., since 1986 and beyond 2005) in the northern

<sup>2</sup> If the most blue-shifted maser(s) would be in the center and the NH<sub>3</sub> velocity signature would have a regular C shape (Ho et al. 1991), this would have been the front side, propagating toward the observer.

part of the disk (YZ96; K03; this work). Previously, only in 1986 a faint, conjugate  $-132$  km s<sup>-1</sup> maser was detected in the southern part of the CND (K03 and references therein) which disappeared before the next possible detection in 1996. Up until now, this single detection has been the only observation suggesting that some 1720 MHz masers are distributed symmetrically in position and velocity with respect to Sgr A\*, like the CND, in sharp contrast to the SNR/ISM interaction at velocities between 30 and 70 km s<sup>-1</sup> as discussed above. The three new detections of high-negative velocity 1720 MHz masers toward the southwestern part of the CND (Table 2) now strongly support the existence of conjugate masers with locations and velocities consistent with originating from gas in the CND. Clearly these masers are variable as they may appear and/or disappear on time scales on the order of years (Sect. 3.1).

The estimated OH column density derived above appears similar across the total extent of the CND, indicating that maser emission potentially could be observed at all azimuthal angles of the CND. This in particular would be the case if Sgr A East would continuously drive planar shocks from behind into the CND while the CND is pushed toward the observer as argued by YZ01 and Lee et al. (2008)<sup>3</sup>. In such a case, one would expect to find some masers originating in the +20 km s<sup>-1</sup> cloud, i.e., with velocities in the  $\sim 10$ – $50$  km s<sup>-1</sup> range, in projection *toward the whole CND*. Though there are three masers in this velocity range north of the CND (and associated with H<sub>2</sub> filaments), there is no distribution toward the rest of the CND. Furthermore, a push from behind would result in a relatively constant pumping of the masers, which due to the clear variability of the southwestern (high-negative velocity) CND masers is hard to support. In contrast, the OH masers in the CND appear only in two regions: slightly east of north and west of south at positions close to the geometrical tangent points. Extended H<sub>2</sub> emission is found nearby those regions, but not distributed in filaments as for the northwestern masers (Sect. 4.3.1). This H<sub>2</sub> emission is due to both limb brightening effects as well as dissipation of shocks in clump-clump interactions (YZ01). For the case of masers in a disk or ring structure, this geometry can be understood by the requirement of having long paths of velocity coherent gas in order to build up a large amplification. Closer to the tangent points of a disk, the path-lengths are longer resulting in a larger amplification (Parra et al. 2005). Such a behavior has previously been observed in maser transitions of H<sub>2</sub>O and OH in extragalactic sources (Miyoshi et al. 1995; Pihlström et al. 2001; Klöckner et al. 2003). It is therefore plausible that the CND masers can be sustained without being a direct result from shocks generated by Sgr A East (Sect. 4.4.2).

##### 4.4.2. Pump source of the CND masers

Whereas the pumping of the SNR masers can be explained by the interaction of the SNR shock plowing into the interstellar material of the +50 km s<sup>-1</sup> cloud, it is not required that the SNR and the CND directly interact to form the CND masers.

A radiative (far-infrared) pump source primarily tends to invert the 1612 MHz line, while collisional excitation has been identified as the prime pumping mechanism for 1720 MHz OH masers (Elitzur 1976). The lack of interstellar OH 1612 MHz and mainline emission in the CND (K03) argues against far-infrared pumping and for a collisional pumping

<sup>3</sup> Note that the Lee et al. (2008) H<sub>2</sub> data do not properly cover the CND.

scheme of the 1720 MHz CN D masers. In the CN D we find extended shock excited  $H_2$  emission in the ‘‘Lobes’’ (YZ01), but not in large-scale shock-front filamentary structure as for the northwestern masers. The clumpiness and irregular distribution of molecular gas in the CN D imply the possibility of frequent clump-clump collisions which could provide the source of a collisional maser pump. The dense ( $n_{H_2} \simeq 3\text{--}4 \times 10^7 \text{ cm}^{-3}$ ) molecular clumps defined by HCN and  $HCO^+$  observations are found more or less in the same locations where bright  $H_2$  emission has been mapped (Wright et al. 2001; Christopher et al. 2005; Jackson et al. 1993; YZ01). YZ01 use the  $H_2$  line emission associated with the CN D to argue that dissipation of the random motions of molecular clumps is the most likely cause of the excitation of the  $H_2$  molecules via shocks, implying the presence of C-type shocks within the CN D. Similar to the C-shock chemistry predicted for SNR/ISM masers, the post-shock regions in the CN D should produce suitable conditions for regions of enhanced OH abundances (Wardle 1999).

Comparing the maser positions with respect to the  $H_2$  (YZ01) and HCN emission (Christopher et al. 2005) and assuming that the CN D masers are excited via shocks, it is not surprising to see a correlation between the maser emission and the  $H_2$  emission. It is interesting to note that the masers always appear to be offset from, and trailing the brightest HCN and  $H_2$  peaks. At the high densities ( $n_{H_2} \sim 10^7 \text{ cm}^{-3}$ ) traced by HCN, maser emission will be quenched. Instead, the masers occur in lower density post-shock regions following/trailing the clumps. The large dispersion ( $\sim 40 \text{ km s}^{-1}$ ) in the southwestern CN D masers may reflect the dispersion of individual clumps in the CN D.

A clumpy medium also appears to be a better maser amplifier than a smooth medium. Extragalactic OH masers have successfully been modeled assuming a clumpy medium (Pihlström et al. 2001; Parra et al. 2005). Modeling of masers in a clumpy medium predicts high maser variability caused by smaller regions of inverted gas moving in and out of the line-of-sight. However, no clear limits could be set on the variability of individual maser features presented in this paper as each observation so far has very different observing parameters (Table 1). A forthcoming paper will properly address the maser variability using homogeneous data sets.

## 5. SUMMARY

The velocities and locations of most 1720 MHz OH masers observed in the GC agree with the commonly adopted model in which the masers arise in regions where the supernova remnant Sgr A East is interacting with the  $+20$  and  $+50 \text{ km s}^{-1}$  molecular clouds and the nearby SNR G359.02–0.09. In addition to extending the database of such masers, in particular toward the interaction region toward the northeast rim of Sgr A East, we have explored the slightly different possible origins of the maser groups, notably the masers northwest of the CN D. We showed that they indicate a region of shock interaction of the near side of Sgr A East with molecular cloud material extending well over the projected size of the CN D. The newly found masers in the northeast indicate such an interaction on the far side of Sgr A East.

Furthermore, we have verified the existence of high-negative velocity masers, which together with previously detected high-positive velocity masers bracket Sgr A\* both in position and velocity. Their positions and velocities are consistent with being located near the tangent points of the CN D. However, we find no need for the SNR to interact directly with the CN D to pump and sustain these high-velocity masers. OH absorption data show that the CN D and Sgr A East are separated by molecular cloud material, and therefore the SNR shock is unlikely to be responsible for pumping these high-velocity masers. Instead a more likely pumping mechanism is by collisions from dissipation between clumps *in* the CN D.

These results imply that 1720 MHz OH masers *not only* do occur in SFRs and in SNR/ISM (and SNR/SNR) interactions, but can also arise in clumpy and disturbed circumnuclear disks at small radii. If sufficiently bright, such 1720 MHz masers could serve as an additional molecular line tool to study circumnuclear gas dynamics around galaxy centers.

## ACKNOWLEDGMENTS

We would like to thank M. Elitzur and V. Fish for their most useful comments on an earlier version of the manuscript, and also S. Stolovy and M. Christopher for kindly sharing their  $H_2$  and HCN maps for reference. The Very Large Array is operated by the National Radio Astronomy Observatory, which is a facility of the National Science Foundation operated under cooperative agreement by Associated Universities, Inc.

*Facility:* VLA

## REFERENCES

- Baudry, A., Diamond, P.J., Booth, R.S., Graham, D., & Walmsley, C. 1988, *A&A*, 201, 105  
 Christopher, M.H., Scoville, N.Z., Stolovy, S.R., & Yun, M.S. 2005, *ApJ*, 622, 346  
 Cohen, R.J., Mashedier, M.R.W., & Caswell, J.L. 1995, *MNRAS*, 274, 808  
 Coil, A.L., & Ho, P.T.P. 2000, *ApJ*, 533, 245  
 Ekers, R.D., van Gorkom, J.H., Schwarz, U.J., & Goss, W.M. 1983, *A&A*, 122, 143  
 Elitzur, M. 1976, *ApJ*, 203, 124  
 Frail, D.A., Goss, W.M., & Slysh, V.I. 1994, *ApJ*, 424, L111  
 Gatley I., Jones T.J., Hyland A.R., Wade R., Geballe T.R., & Krisciunas K. 1986, *MNRAS*, 222, 299  
 Gray, M.D., Doel, R.C., & Field, D. 1991, *MNRAS*, 252, 30  
 Gray, M.D., Field, D., & Doel, R.C. 1992, *A&A*, 262, 555  
 Green, A.J., Frail, D.A., Goss, W.M., & Otrupcek, R. 1997, *AJ*, 114, 2058  
 Guesten, R., Walmsley, C.M., & Pauls, T. 1981, *A&A*, 103, 197  
 Herrnstein, R.M., & Ho, P.T. 2005, *ApJ*, 620, 287  
 Ho, P.T.P., Jackson, J.M., Barrett, A.H., & Armstrong, J.T. 1985, *ApJ*, 288, 575  
 Ho, P.T.P., Ho, L.C., Szczepanski, J.C., Jackson, J.M., & Armstrong, J.T. 1991, *Nature*, 350, 309  
 Jackson, J.M. et al. 1993, *ApJ*, 402, 173  
 Karlsson, R., Sjouwerman, L.O., Sandqvist, A., & Whiteoak, J.B. 2003, *A&A*, 403, 1011 (K03)  
 Klöckner, H.-R., Baan, W.A., & Garrett, M.A. 2003, *Nature*, 421, 821  
 Lee, S., Pak, S., Davis, C.J., Herrnstein, R.M., Geballe, T.R., Ho, P.T.P., & Wheeler, J.C. 2003, *MNRAS*, 341, 509  
 Lee, S., et al., 2008, *ApJ*, 674, 247  
 Lockett, P., Gauthier, E., & Elitzur, M. 1999, *ApJ*, 511, L235  
 Marshall J., Lasenby A.N., & Harris A.I. 1995, *MNRAS*, 277, 594  
 McGary, R.S., Coil, A.L., & Ho, P.T. 2001, *ApJ*, 559, 326  
 Mezger, P.G., Duschl, W.J., & Zylka, R. 1996, *A&A Rev.*, 7, 289  
 Morris, M., & Serabyn, E. 1996, *ARA&A*, 34, 645  
 Miyoshi, M., Moran, J., Herrnstein, J., Greenhill, L., Nakai, N., Diamond, P., & Makoto, I. 1995, *Nature*, 373, 127  
 Niezurawska, A., Szymczak, M., Richards, A.M.S., & Cohen, R.J. 2004, *MNRAS*, 350, 1409  
 Nord, M.E., Lazio, T.J.W., Kassim, N.E., Goss, W.M., & Duric, N. 2004, *ApJ*, 601, L51  
 Palmer, P., Gardner, F.F., & Whiteoak, J.B. 1984, *MNRAS*, 211, 41  
 Parra, R., Conway, J.E., Elitzur, M., & Pihlström, Y.M. 2005, *A&A*, 443, 383  
 Pavlakis, K.G., & Kylafis, N.D. 1996, *ApJ*, 467, 300  
 Pedlar, A., Anantharamaiah, K.R., Ekers, R.D., Goss, W.M., van Gorkom, J.H., Schwarz, U.J., & Zhao, J.-H. 1989, *ApJ*, 342, 769

- Pihlström, Y.M., & Sjouwerman, L.O. 2006, JPhCS, 54, 77  
Pihlström, Y.M., Conway, J.E., Booth, R.S., Diamond, P.J., & Polatidis, A.G. 2001, A&A, 377, 413  
Pihlström, Y.M., Fish, V.L., Sjouwerman, L.O., Zschaechner, L.K., Lockett, P.B., & Elitzur, M. 2008, ApJ, 676, 371  
Reid, M. J., & Brunthaler, A. 2004, ApJ, 616, 872  
Sakano, M., Warwick, R.S., Decourchelle, A., & Predehl, P. 2003, MNRAS, 340, 747  
Sandqvist Aa. 1970, AJ, 75, 135  
Sandqvist Aa. 1974, A&A, 33, 413  
Sandqvist, Aa. 1989, A&A, 223, 293  
Szymczak, M., & Gérard, E. 2004, A&A, 414, 235  
Tsuboi M., Okumura S.K., Miyazaki A. 2006, JPhCS, 54, 16  
Vollmer, B., Zylka, R., & Duschl, W. J. 2003, A&A, 407, 515  
Wardle, M. 1999, ApJ, 525, L101  
Wright, M.C.H., Coil, A.L., McGary, R.S., Ho, P.T.P. & Harris, A.I. 2001, ApJ, 551, 254  
Yusef-Zadeh, F., Roberts, D.A., Goss, W.M., Frail, D.A., & Green, A.J. 1996, ApJ, 466, L25 (YZ96)  
Yusef-Zadeh, F., Roberts, D.A., Goss, W.M., Frail, D.A., & Green, A.J. 1999, ApJ, 512, 230  
Yusef-Zadeh, F., Stolovy, S.R., Burton, M., Wardle, M., & Ashley, M.C.B. 2001, ApJ, 560, 749 (YZ01)  
Whiteoak, J.B., Rogstad, D.H., & Lockhart, I.A. 1974, A&A, 36, 245  
Zylka, R., Mezger, P.G., & Wink, J.E. 1990, A&A, 234, 133